chemistry

MDPI

Article

Structures and Bonding in Hexacarbonyl Diiron Polyenes: Cycloheptatriene and 1,3,5-Cyclooctatriene

Min Zhang [1] and Guangchao Liang [2,*]

[1] Department of Pharmacy, School of Medicine, Xi'an International University, Xi'an 710077, China; zhangmin01@xaiu.edu.cn
[2] Academy of Advanced Interdisciplinary Research, Xidian University, Xi'an 710071, China
* Correspondence: liangguangchao@xidian.edu.cn

Abstract: Structural preferences of (1,3,5-cyclooctatriene) hexacarbonyl diiron [$(C_8H_{10})Fe_2(CO)_6$] and cycloheptatriene hexacarbonyl diiron [$(C_7H_8)Fe_2(CO)_6$] were explored using density functional theory (DFT) computations. DFT computations together with experimental results demonstrated that structure with the [η^3, (η^1, η^2)] mode is the preferred structure in $(C_8H_{10})Fe_2(CO)_6$, and the [η^3,η^3] mode is preferred in $(C_7H_8)Fe_2(CO)_6$. For $(C_8H_{10})Fe_2(CO)_6$, the conversion between the structures with [η^3, (η^1, η^2)] mode and the [η^3, η^3] mode is prevented by the relatively high activation barrier. $(C_8H_{10})Fe_2(CO)_6$ is indicated as a fluxional molecule with a Gibbs free energy of activation of 8.5 kcal/mol for its ring flicking process, and an excellent linear correlation (R^2 = 0.9909) for the DFT simulated ^{1}H-NMR spectra was obtained. Results provided here will develop the understanding on the structures of other polyene analogs.

Keywords: diiron polyene; DFT computation; fluxionality; ring flicking

Citation: Zhang, M.; Liang, G. Structures and Bonding in Hexacarbonyl Diiron Polyenes: Cycloheptatriene and 1,3,5-Cyclooctatriene. *Chemistry* **2022**, *4*, 447–453. https://doi.org/10.3390/chemistry4020033

Academic Editor: Maxim L. Kuznetsov

Received: 27 April 2022
Accepted: 13 May 2022
Published: 15 May 2022

Publisher's Note: MDPI stays neutral with regard to jurisdictional claims in published maps and institutional affiliations.

1. Introduction

In the early 1960s, two structures of (1,3,5-cyclooctatriene) hexacarbonyl diiron [$(C_8H_{10})Fe_2(CO)_6$] with different bonding modes based on the ^{1}H-NMR spectrum ([η^4, η^2] mode of **TS-3** in Scheme 1) and the Mössbauer absorption spectrum ([η^3, η^3] mode of **2** in Scheme 1) were proposed [1,2]. Subsequently, a reported X-ray crystal structure of $(C_8H_{10})Fe_2(CO)_6$ [3] showed that the correct bonding of $(C_8H_{10})Fe_2(CO)_6$ displayed a special [η^3, (η^1, η^2)] mode (**1** in Scheme 1), not the [η^4, η^2] or [η^3, η^3] mode, and this [η^3, (η^1, η^2)] mode was also believed to be the preferred structure in solution [3].

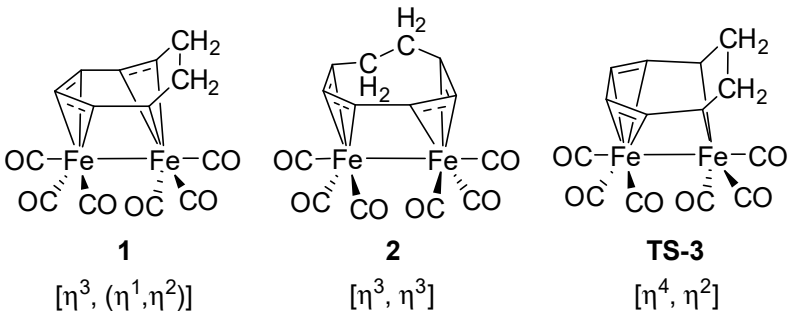

Scheme 1. Possible structures of $(C_8H_{10})Fe_2(CO)_6$.

The variable temperature (from −107 °C to 28 °C) ^{1}H-NMR spectra of $(C_8H_{10})Fe_2(CO)_6$ indicated it was a fluxional molecule [4], which could undergo rapidly flicking back and forth, similar to a windshield wiper (structure **TS-3** in Scheme 1) [4,5]. The high-temperature coalescence of the two mirror isomers (1 and 1*i*) through the C_s symmetrical transition state yielded only five proton peaks in the ^{1}H-NMR spectrum, with relative

intensities of 2:2:2:2:2. The C_1 symmetrical complex with [η^3, η^3] mode (**2** in Scheme 1) was suggested as a possible higher energetic minimum compared with the complex with [η^3, (η^1, η^2)] mode (**1** in Scheme 1), and the C_s symmetrical complex with [η^4, η^2] mode (**TS-3** in Scheme 1) was suggested as a possible transition state. However, it is surprising that the X-ray crystal structure of the 1,3,5-cyclooctatriene homologous analog, cycloheptatriene hexacarbonyl diiron [$(C_7H_8)Fe_2(CO)_6$], exhibited a [η^3, η^3] mode [6], instead of the [η^3, (η^1, η^2)] mode in $(C_8H_{10})Fe_2(CO)_6$. As the homologous series of cyclopolyene, a similar bonding mode of the 1,3,5-cyclooctatriene (C_8H_{10}) and cycloheptatriene (C_7H_8) hexacarbonyl diiron complexes could be expected. The observed different bonding modes suggested that $(C_8H_{10})Fe_2(CO)_6$ may have two different ground state minima ([η^3, η^3] mode and [η^3, (η^1, η^2)] mode), and the conversion between these two minima is prohibited by the high activation barrier. Two different ground state minima ([η^3, η^3] mode and [η^3, (η^1, η^2)] mode) may also exist for $(C_7H_8)Fe_2(CO)_6$, but the conversion between these two minima is also limited by the relatively high activation barrier. These special coordination modes and related transformations were also observed in the cyclooctatetraene-coordinated diiron complex and cyclooctatriene-coordinated Ru complex [7,8].

Here, the density functional theory (DFT) computations were performed to study the structures and bonding of $(C_7H_8)Fe_2(CO)_6$ and $(C_8H_{10})Fe_2(CO)_6$. To investigate the different bonding modes presented in Scheme 1, the possible dynamic fluxional processes of $(C_7H_8)Fe_2(CO)_6$ and $(C_8H_{10})Fe_2(CO)_6$ were explored, and the variable-temperature ^{1}H-NMR spectra were also simulated. Results provided here could benefit the understanding on the structures of other cyclopolyene analogs.

2. Computational Methods

Gas-phase geometry optimizations using the Gaussian 09 package [9] were carried out with PBEPBE [10] functional and density fitting approximation [11,12] (keyword AUTO), employing the modified-LANL2DZ with the *f* polarization (modified-LANL2DZ(*f*)) [13–15] and the effective core potential (ECP, LANL2DZ) for Fe atoms, employing LANL2DZ(*d*, *p*) [16,17] with the related ECP (LANL2DZ) for Si atoms in the reference system TMS, and employing the 6-31G (*d*′) [18–20] basis sets for all other atoms (C, O, and H) (BS1). The accuracy and reliability of the computational methodology had been demonstrated by previous studies on organometallic complexes [21–23]. Vibrational frequency computations were used to verify the natures of all stationary points. All located transition states were obtained with only one imaginary frequency, and minima without any imaginary frequencies were obtained [21,24]. Spherical harmonic 5*d* and 7*f* functions and the pruned fine integration grids with 75 radial shells and 302 angular points per shell were used for all computations. Free energy corrections were performed at 1 atm and 298.15 K.

^{1}H-NMR computations were carried out using the gauge-independent atomic orbital (GIAO) method [25–27] with PBEPBE functional and basis sets 2 (BS2), based on gas-phase optimized geometry. In BS2, LANL08(*f*) [14,28] and ECP (LANL2DZ) basis sets were employed for Fe, LANL08(*d*) [17,28] and related ECP (LANL2DZ) for Si, and the 6-311G++(3*df*, 3*pd*) [29,30] basis sets for other atoms (C, O, and H). All simulated proton chemical shifts were relative to the absolute shift of TMS (calc. 31.03 ppm).

3. Results and Discussion

The DFT-optimized structures of $(C_7H_8)Fe_2(CO)_6$ and $(C_8H_{10})Fe_2(CO)_6$ were compared with their experimental X-ray structures (CSD entries: CYHPFE and CYOFEC). The RMSD values (in Å, without hydrogens) for $(C_7H_8)Fe_2(CO)_6$ and $(C_8H_{10})Fe_2(CO)_6$) are 0.0495 and 0.056, respectively (Figure 1, Table S1), which demonstrated the good performance of the computational methodology [21,31,32]. Previous studies have suggested that $(C_8H_{10})Fe_2(CO)_6$ is a fluxional molecule undergoing several dynamic interconversions and $(C_7H_8)Fe_2(CO)_6$ is not a fluxional molecule. The possible dynamic processes of $(C_8H_{10})Fe_2(CO)_6$ and $(C_7H_8)Fe_2(CO)_6$ are examined in the following sections.

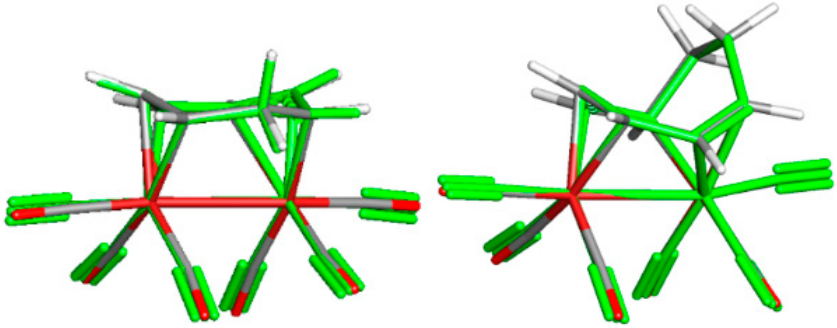

Figure 1. Overlaid structures of the X-ray crystal (green) and optimized structures of $(C_7H_8)Fe_2(CO)_6$ (left) and $(C_8H_{10})Fe_2(CO)_6$ (right). Color code: red, Fe; gray, C; red, O; white, H.

3.1. The Interconversions of $(C_7H_8)Fe_2(CO)_6$

Comparisons of the computed Gibbs free energies of structures with [η^3, η^3] mode and [η^3, (η^1, η^2)] mode (0.0 vs. 4.9, in kcal/mol, Figure 2) showed that structure with the [η^3, η^3] mode is demonstrated as the preferred structure of $(C_7H_8)Fe_2(CO)_6$, which is consistent with the experimental X-ray crystal structure [6]. DFT optimized structure with the C_s symmetrical [η^3, η^3] mode was proven as a transition state (TS-1 in Figure 2, 1.4 kcal/mol), which connected two mirror isomers of the C_1 symmetrical [η^3, η^3] complex. The tricarbonyl equivalence process with a Gibbs barrier of 9.6 kcal/mol (TS-2 in Figure 2) was also located. To explore the possible dynamic processes of $(C_7H_8)Fe_2(CO)_6$, a conversion between [η^3, η^3] mode complex **1** and [η^3, (η^1,η^2)] mode complex **2** was performed. No direct conversion between complex **1** and complex **2** could be obtained, and a two-step conversion through bridging CO [μ_2-η^4, η^2] complex **3** (16.3 kcal/mol) was located. Relatively high Gibbs barriers for the conversion between complex **1** with the [η^3, η^3] mode and complex **3** with the [μ_2-η^4, η^2] mode (17.8 kcal/mol), and conversion between complex **3** and complex **2** with the [η^3, (η^1, η^2)] mode (21.3 kcal/mol) were obtained, which prevented low-temperature conversion between [η^3, η^3] mode complex **1** and [η^3, (η^1, η^2)] mode complex **2**.

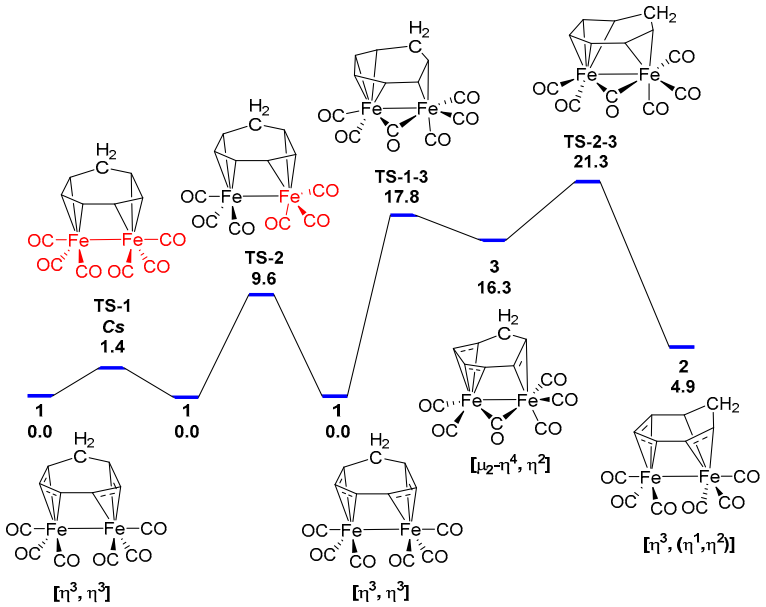

Figure 2. Interconversions of the C_1 symmetrical $(C_7H_8)Fe_2(CO)_6$. All Gibbs energies are relative to complex **1**.

3.2. Dynamic Fluxionality of $(C_8H_{10})Fe_2(CO)_6$

In contrast to the preferred structure with [η^3, η^3] mode in $(C_7H_8)Fe_2(CO)_6$, structure with [η^3, (η^1, η^2)] mode (complex **1** in Figure 3, 0.0 kcal/mol)of $(C_8H_{10})Fe_2(CO)_6$ was more favorable than the structure with [η^3, η^3] mode (complex **2** in Figure 3, 12.0 kcal/mol) [3]. The Fe–Fe bond length in complex **1** with the [η^3, (η^1, η^2)] mode in $(C_8H_{10})Fe_2(CO)_6$ was 2.766 Å, which is similar to that in $(C_7H_8)Fe_2(CO)_6$ ($d_{(Fe\text{-}Fe)}$ = 2.767 Å). However, the Fe–Fe bond length in complex **2** with the [η^3, η^3] mode ($d_{(Fe\text{-}Fe)}$ = 2.932 Å) in $(C_8H_{10})Fe_2(CO)_6$ was longer than that of $(C_7H_8)Fe_2(CO)_6$ ($d_{(Fe\text{-}Fe)}$ = 2.868 Å) due to an additional methylene fragment. The (Fe–CH–CH_2–CH_2–CH) five-member ring in the complex **1** with [η^3, (η^1, η^2)] mode of $(C_8H_{10})Fe_2(CO)_6$ caused the structural preference, as opposed to the (Fe-CH-CH_2-CH) four-member ring in the complex with [η^3, (η^1, η^2)] mode of $(C_7H_8)Fe_2(CO)_6$. It is worth noting that the Gibbs free energy difference between the [η^3, η^3] mode and [η^3, (η^1, η^2)] mode of $(C_8H_{10})Fe_2(CO)_6$ was much higher than that of $(C_7H_8)Fe_2(CO)_6$ (12.0 kcal/mol vs. 4.9 kcal/mol). Three different dynamic processes, including two tricarbonyl equivalence processes (9.1 kcal/mol for C_1 symmetrical TS-1 and 14.2 kcal/mol for C_1 symmetrical TS-2) and one ring flicking process (8.5 kcal/mol C_s symmetrical **TS-3**), were found in the interconversion of [η^3, (η^1, η^2)] mode complex **1** (and enantiomer 1*i*) of $(C_8H_{10})Fe_2(CO)_6$. The experimental variable-temperature NMR spectra of $(C_8H_{10})Fe_2(CO)_6$ were not well resolved, but the activation energy for the ring flicking process was roughly estimated from 10.3 kcal/mol to 11.6 ± 2 kcal/mol [4,33,34], which was close to the DFT-computed values (8.5 kcal/mol for **TS-3**). The equivalence process of asymmetric [η^1, η^2]-$Fe(CO)_3$ rotation (TS-2, 14.2 kcal/mol) had a higher rotation barrier compared with the symmetric η^3-$Fe(CO)_3$ rotation (TS-1, 9.1 kcal/mol), which was in agreement with experimental observations (15.6 ± 2 kcal/mol for asymmetric and 11.4 ± 2 kcal/mol for symmetric process) [33]. A direct conversion between [η^3, (η^1, η^2)] mode complex **1** and [η^3, η^3] mode complex **2** of $(C_8H_{10})Fe_2(CO)_6$ was located, and the Gibbs barrier was 28.7 kcal/mol (TS-1-2, Figure 3). Indirect conversion through bridging CO [μ_2-η^4, η^2] complex **3** (24.9 kcal/mol) was also achieved. Relatively high Gibbs barriers for the conversions between complex **1i** and complex **3** (26.2 kcal/mol) and between complex **3** and complex **2** (26.1 kcal/mol) were obtained.

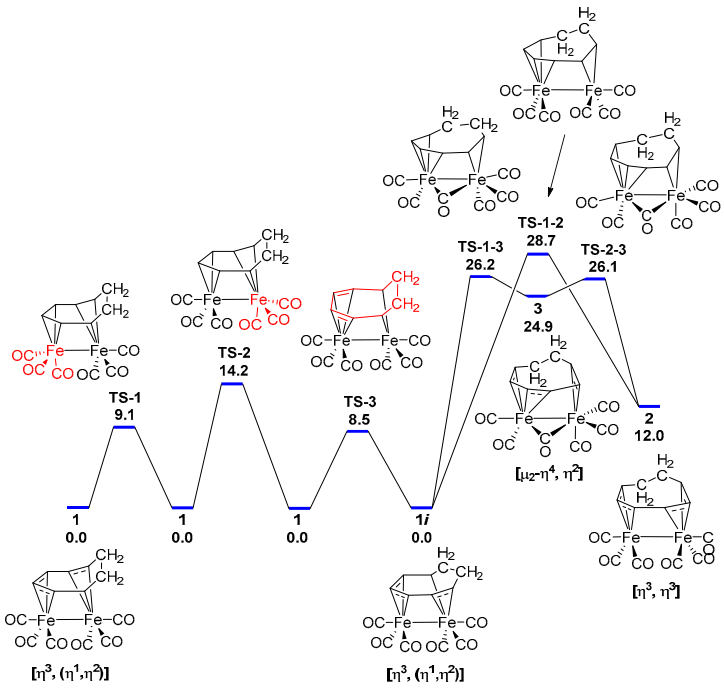

Figure 3. Free energy diagram of $(C_8H_{10})Fe_2(CO)_6$. All Gibbs energies are relative to complex **1**.

3.3. Interpretations of the Dynamic Fluxionality

The relatively high activation energies of $(C_7H_8)Fe_2(CO)_6$ (21.3 kcal/mol of TS-2-3, Figure 2) and $(C_8H_{10})Fe_2(CO)_6$ (26.1 kcal/mol of TS-2-3, Figure 3) indicated that the conversion between the structures of [η^3, (η^1, η^2)] mode and [η^3, η^3] mode cannot occur under experimental conditions. The C_s symmetrical TS-1 and tricarbonyl equivalence process TS-2 of $(C_7H_8)Fe_2(CO)_6$ could not affect the proton peak pattern in the ^{1}H-NMR spectra; therefore, $(C_7H_8)Fe_2(CO)_6$ was assigned as a non-fluxional molecule. In contrast, $(C_8H_{10})Fe_2(CO)_6$ was assigned as a fluxional molecule. The C_s symmetrical **TS-3** ring flicking in complex **1** with [η^3, (η^1, η^2)] mode of $(C_8H_{10})Fe_2(CO)_6$ could change the patterns of proton peaks in the variable-temperature ^{1}H-NMR spectra. At the low-temperature limit, the chemical environments of the 10 protons in $(C_8H_{10})Fe_2(CO)_6$ are different. No equivalent proton exists at the low-temperature limit, and 10 proton peaks are shown in the ^{1}H-NMR spectrum at a 1:1:1:1:1:1:1:1:1:1 ratio. When the temperature was raised, the C_s symmetrical [η^4, η^2] mode transition states TS-2 generates five proton peaks in the ^{1}H-NMR spectrum at a 2:2:2:2:2 ratio (Table S2) [4]. The gas phase variable-temperature ^{1}H-NMR spectra of $(C_8H_{10})Fe_2(CO)_6$ and $(C_7H_8)Fe_2(CO)_6$ were simulated (Figure 4, Figures S1 and S2, Table S2). An excellent linear relationship (R^2 = 0.9909) between the DFT-computed proton chemical shifts and the experimental ^{1}H-NMR (Figure 5) of $(C_8H_{10})Fe_2(CO)_6$ was achieved.

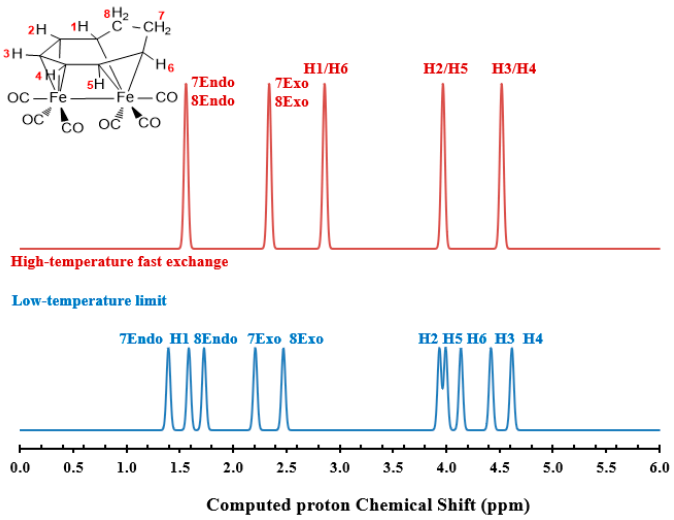

Figure 4. Simulated gas phase ^{1}H-NMR spectra of $(C_8H_{10})Fe_2(CO)_6$ at the low-temperature limit (bottom, blue) and high-temperature fast exchange (top, red).

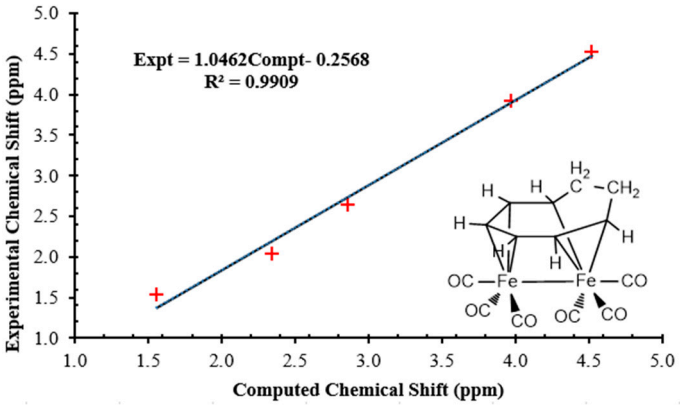

Figure 5. Linear fitting between the computed gas phase proton chemical shifts and experimental ^{1}H-NMR of $(C_8H_{10})Fe_2(CO)_6$.

4. Conclusions

Reactions of cyclopolyene with iron carbonyls could generate various diiron complexes, which usually contain serval different bonding modes. To provide a straightforward understanding on the change in hapticity, DFT computations were carried out to explore the structural preferences of (1, 3, 5-cyclooctatriene) hexacarbonyl diiron [$(C_8H_{10})Fe_2(CO)_6$] and cycloheptatriene hexacarbonyl diiron [$(C_7H_8)Fe_2(CO)_6$]. The computational results showed that the two bridging ethylene fragments (-CH_2-CH_2-) in $(C_8H_{10})Fe_2(CO)_6$ made the structure with the [η^3, (η^1, η^2)] mode favorable, other than the [η^3, η^3] mode in $(C_7H_8)Fe_2(CO)_6$. C_s symmetrical ring flicking (**TS-3**, 8.5 kcal/mol) was the dominant factor in the interconversions of the structure with the [η^3, (η^1, η^2)] mode of $(C_8H_{10})Fe_2(CO)_6$. The gas-phase ^{1}H-NMR spectra of $(C_8H_{10})Fe_2(CO)_6$ were simulated based on the dominant C_s symmetrical **TS-3** ring flicking, which showed excellent correlation (R^2 = 0.9909) between the computed gas-phase proton chemical shifts and experimental ^{1}H-NMR of $(C_8H_{10})Fe_2(CO)_6$. Transition metal complexes with cyclopolyene ligands are widely used as the starting materials in synthesis and photochemical studies, and interpretations of the bonding modes of [$(C_7H_8)Fe_2(CO)_6$] and $(C_8H_{10})Fe_2(CO)_6$ from this study could provide some basic insights on the structures of other transition metal cyclopolyene analogs.

Supplementary Materials: The following supporting information can be downloaded at: https://www.mdpi.com/article/10.3390/chemistry4020033/s1, Table S1. Selected bond lengths and angles; Table S2. Computed proton chemical shifts; Figure S1. Simulated gas phase ^{1}H-NMR spectra; Figure S2. Linear fitting; Table S3. Cartesian coordinates of optimized structures.

Author Contributions: M.Z.: investigation, formal analysis, writing—original draft; G.L.: conceptualization, investigation, formal analysis, methodology, writing—reviewing and editing, funding acquisition. All authors have read and agreed to the published version of the manuscript.

Funding: This research was supported by start-up funds from Xidian University (1018/10251210050).

Institutional Review Board Statement: Not applicable.

Informed Consent Statement: Not applicable.

Data Availability Statement: Not applicable.

Acknowledgments: We thank the high-performance computing platform of Xidian University (XDHCPP) for computing support. We are grateful for the financial support from the Academy of Advanced Interdisciplinary Research and the start-up funds from Xidian University (1018/10251210050), and support from Xi'an International University.

Conflicts of Interest: The authors declare no conflict of interest.

References

1. King, R.B. Organometallic Chemistry of the Transition Metals. V. New Iron Carbonyl Complexes of Cycloöctatriene Derivatives. *Inorg. Chem.* **1963**, *2*, 807–810. [CrossRef]
2. Emerson, G.F.; Mahler, J.E.; Pettit, R.; Collins, R. Organometallic Complexes of the Type Triene-$Fe_2(CO)_6$. *J. Am. Chem. Soc.* **1964**, *86*, 3590–3591. [CrossRef]
3. Cotton, F.A.; Edwards, W.T. Crystal and molecular structure of (1,3,5-cyclooctatriene)diiron hexacarbonyl. *J. Am. Chem. Soc.* **1969**, *91*, 843–847. [CrossRef]
4. Cotton, F.A.; Marks, T.J. Stereochemically nonrigid organometallic molecules XXV. The low-temperature PMR spectrum of cis-(1,2,6-trihapto:3,4,5-trihapto-1,3,5-cyclooctatriene)hexacarbonyldiiron. *J. Organomet. Chem.* **1969**, *19*, 237–240. [CrossRef]
5. Cotton, F.A. A Half-Century of Nonclassical Organometallic Chemistry: A personal Perspective. *Inorg. Chem.* **2002**, *41*, 643–658. [CrossRef] [PubMed]
6. Cotton, F.A.; DeBoer, B.G.; Marks, T.J. Stereochemically nonrigid organometallic molecules. XXIX. Cycloheptatrienediiron hexacarbonyl. *J. Am. Chem. Soc.* **1971**, *93*, 5069–5075. [CrossRef]
7. Komiya, S.; Planas, J.G.; Onuki, K.; Lu, Z.; Hirano, M. Versatile Coordination Modes and Transformations of the Cyclooctatriene Ligand in Ru(C_8H_{10})L_3 (L = Tertiary Phosphine). *Organometallics* **2000**, *19*, 4051–4059. [CrossRef]
8. Zhang, L.; Zhang, S.; Xu, Q.; Sun, J.; Chen, J. Cyclooctatetraene (COT)-Coordinated Diiron Carbene Complexes and Their Remarkable Thermolysis Reactions. *Organometallics* **2005**, *24*, 933–944. [CrossRef]

9. Frisch, M.J.; Trucks, G.W.; Schlegel, H.B.; Scuseria, G.E.; Robb, M.A.; Cheeseman, J.R.; Scalmani, G.; Barone, V.; Mennucci, B.; Petersson, G.A.; et al. *Gaussian 09, Revision, D.01*; Gaussian, Inc.: Wallingford, CT, USA, 2013.
10. Perdew, J.P.; Burke, K.; Ernzerhof, M. Generalized Gradient Approximation Made Simple. *Phys. Rev. Lett.* **1996**, *77*, 3865–3868, Erratum in *Phys. Rev. Lett.* **1997**, *78*, 1396. [CrossRef]
11. Dunlap, B.I. Fitting the Coulomb potential variationally in Xα molecular calculations. *J. Chem. Phys.* **1983**, *78*, 3140–3142. [CrossRef]
12. Dunlap, B.I. Robust and variational fitting: Removing the four-center integrals from center stage in quantum chemistry. *J. Mol. Struct. THEOCHEM* **2000**, *529*, 37–40. [CrossRef]
13. Couty, M.; Hall, M.B. Basis sets for transition metals: Optimized outer p functions. *J. Comput. Chem.* **1996**, *17*, 1359–1370. [CrossRef]
14. Hay, P.J.; Wadt, W.R. Ab initio effective core potentials for molecular calculations. Potentials for K to Au including the outermost core orbitals. *J. Chem. Phys.* **1985**, *82*, 299–310. [CrossRef]
15. Hay, P.J.; Wadt, W.R. Ab initio effective core potentials for molecular calculations. Potentials for the transition metal atoms Sc to Hg. *J. Chem. Phys.* **1985**, *82*, 270–283. [CrossRef]
16. Check, C.E.; Faust, T.O.; Bailey, J.M.; Wright, B.J.; Gilbert, T.M.; Sunderlin, L.S. Addition of polarization and diffuse functions to the LANL2DZ basis set for p-block elements. *J. Phys. Chem. A* **2001**, *105*, 8111–8116. [CrossRef]
17. Wadt, W.R.; Hay, P.J. Ab initio effective core potentials for molecular calculations. Potentials for main group elements Na to Bi. *J. Chem. Phys.* **1985**, *82*, 284–298. [CrossRef]
18. Hehre, W.J.; Ditchfield, R.; Pople, J.A. Self-Consistent Molecular-Orbital Methods. XII. Further Extensions of Gaussian-Type Basis Sets for Use in Molecular-Orbital Studies of Organic-Molecules. *J. Chem. Phys.* **1972**, *56*, 2257–2261. [CrossRef]
19. Hariharan, P.C.; Pople, J.A. Influence of Polarization Functions on Molecular-Orbital Hydrogenation Energies. *Theor. Chim. Acta* **1973**, *28*, 213–222. [CrossRef]
20. The 6-31G(d′) Basis Set Has the Exponent of D Polarization Functions for C, N, O, and F Taken from the 6-311G(d) Basis Sets, Instead of the Original Arbitrarily Assigned Exponent of 0.8 Used in the 6-31G(d) Basis Sets. For H, the 6-31G(d′) Keyword Utilizes the 6-31G(d) Basis Sets.
21. Liang, G.; Webster, C.E. The Missing Agostomer in the Fluxionality of Cyclohexenyl Manganese Tricarbonyl. *J. Organomet. Chem.* **2018**, *864*, 128–135. [CrossRef]
22. Novikov, A.S.; Kuznetsov, M.L. Theoretical study of Re(IV) and Ru(II) bis-isocyanide complexes and their reactivity in cycloaddition reactions with nitrones. *Inorg. Chim. Acta* **2012**, *380*, 78–89. [CrossRef]
23. Novikov, A.S.; Kuznetsov, M.L.; Rocha, B.G.M.; Pombeiro, A.J.L.; Shul'pin, G.B. Oxidation of olefins with H_2O_2 catalysed by salts of group III metals (Ga, In, Sc, Y and La): Epoxidation versus hydroperoxidation. *Catal. Sci. Technol.* **2016**, *6*, 1343–1356. [CrossRef]
24. Liang, G.; Hollis, T.K.; Webster, C.E. Computational Analysis of the Intramolecular Oxidative Amination of an Alkene Catalyzed by the Extreme π-loading N-Heterocyclic Carbene Pincer Tantalum(V) Bis(imido) Complex. *Organometallics* **2018**, *37*, 1671–1681. [CrossRef]
25. Ditchfield, R. Self-consistent perturbation theory of diamagnetism. 1. Gauge-invariant LCAO method for N.M.R. chemical shifts. *Mol. Phys.* **1974**, *27*, 789–807. [CrossRef]
26. Wolinski, K.; Hilton, J.F.; Pulay, P. Efficient Implementation of the Gauge-Independent Atomic Orbital Method for NMR Chemical Shift Calculations. *J. Am. Chem. Soc.* **1990**, *112*, 8251–8260. [CrossRef]
27. Cheeseman, J.R.; Trucks, G.W.; Keith, T.A.; Frisch, M.J. A Comparison of Models for Calculating Nuclear Magnetic Resonance Shielding Tensors. *J. Chem. Phys.* **1996**, *104*, 5497–5509. [CrossRef]
28. Roy, L.E.; Hay, P.J.; Martin, R.L. Revised basis sets for the LANL effective core potentials. *J. Chem. Theory Comput.* **2008**, *4*, 1029–1031. [CrossRef]
29. Krishnan, R.; Binkley, J.S.; Seeger, R.; Pople, J.A. Self-consistent molecular orbital methods. XX. A basis set for correlated wave functions. *J. Chem. Phys.* **1980**, *72*, 650–654. [CrossRef]
30. Frisch, M.J.; Pople, J.A.; Binkley, J.S. Self-Consistent Molecular-Orbital Methods. 25. Supplementary Functions for Gaussian-Basis Sets. *J. Chem. Phys.* **1984**, *80*, 3265–3269. [CrossRef]
31. Gericke, R.; Wagler, J. Ruthenium Complexes of Stibino Derivatives of Carboxylic Amides: Synthesis and Characterization of Bidentate Sb,E, Tridentate Sb,E_2, and Tetradentate Sb,E_3 (E = N and O) Ligands and Their Reactivity Toward $[RuCl_2(PPh_3)_3]$. *Inorg. Chem.* **2020**, *59*, 6359–6375. [CrossRef]
32. Škríba, A.; Jašík, J.; Andris, E.; Roithová, J. Interaction of Ruthenium(II) with Terminal Alkynes: Benchmarking DFT Methods with Spectroscopic Data. *Organometallics* **2016**, *35*, 990–994. [CrossRef]
33. Cotton, F.A.; Hunter, D.L. Carbon-13 nuclear magnetic resonance study of the fluxional character of the .eta.6-(bicyclo[6.2.0]dodeca-2,4,6-triene)hexacarbonyldiiron(Fe-Fe) and a triethylphosphine derivative thereof, and the crystal structure of the latter. *J. Am. Chem. Soc.* **1975**, *97*, 5739–5746. [CrossRef]
34. Deganello, G.; Lewis, J.; Parker, D.G.; Sandrini, P.L. The fluxional behaviour of η6(bicyclo[6.2.0]deca-2,4,6-triene) hexacarbonyl diruthenium (Ru-Ru) by 1H and 13C-NMR techniques. *Inorg. Chem. Acta* **1977**, *24*, 165–171. [CrossRef]